The Astrophysical Journal, 752:29 (10pp), 2012 June 10 doi:10.1088/0004-637X/752/1/29

ICECUBE NONDETECTION OF GAMMA-RAY BURSTS: CONSTRAINTS ON THE FIREBALL PROPERTIES

Hao-Ning He[1,2,3], Ruo-Yu Liu[1,2], Xiang-Yu Wang[1,2], Shigehiro Nagataki[3], Kohta Murase[4], and Zi-Gao Dai[1,2]
[1] School of Astronomy and Space Science, Nanjing University, Nanjing 210093, China; haoninghe@nju.edu.cn, ryliu@nju.edu.cn, xywang@nju.edu.cn
[2] Key Laboratory of Modern Astronomy and Astrophysics (Nanjing University), Ministry of Education, Nanjing 210093, China
[3] Yukawa Institute for Theoretical Physics, Kyoto University, Oiwakecho, Kitashirakawa, Sakyoku, Kyoto 606-8502, Japan
[4] Department of Physics, Center for Cosmology and AstroParticle Physics, The Ohio State University, Columbus, OH 43210, USA
Received 2012 February 19; accepted 2012 April 5; published 2012 May 23

ABSTRACT

The increasingly deep limit on the neutrino emission from gamma-ray bursts (GRBs) with IceCube observations has reached a level that could place useful constraints on the fireball properties. We first present a revised analytic calculation of the neutrino flux that predicts a flux of one order of magnitude lower than that obtained by the IceCube Collaboration. For the benchmark model parameters (e.g., the bulk Lorentz factor is $\Gamma = 10^{2.5}$, the observed variability time for the long GRBs is $t_v^{\rm ob} = 0.01$ s, and the ratio between the energy in the accelerated protons and in the radiation is $\eta_p = 10$ for every burst) in the standard internal shock scenario, the predicted neutrino flux from 215 bursts during the period of the 40- and 59-string configurations is a factor of $\sim$3 below the IceCube sensitivity. However, if we accept the recently found inherent relation between the bulk Lorentz factor and the burst energy, then the expected neutrino flux significantly increases and the spectral peak shifts to a lower energy. In this case, the nondetection implies that the baryon-loading ratio should be $\eta_p \lesssim 10$ if the variability time of the long GRBs is fixed to $t_v^{\rm ob} = 0.01$ s. Instead, if we relax the standard internal-shock scenario but still assume $\eta_p = 10$, then the nondetection constrains the dissipation radius, $R \gtrsim 4 \times 10^{12}$ cm, assuming the same dissipation radius for every burst and benchmark parameters for the fireballs. We also calculate the diffuse neutrino flux from the GRBs for different luminosity functions from the literature. The expected flux exceeds the current IceCube limit for some of the luminosity functions, and, thus, the nondetection constrains $\eta_p \lesssim 10$ when the variability time of the long GRBs is fixed at $t_v^{\rm ob} = 0.01$ s.

Key words: gamma-ray burst: general – neutrinos

Online-only material: color figures

1. INTRODUCTION

Gamma-ray bursts (GRBs) have been proposed as one of the potential sources for ultra-high energy cosmic rays (UHECRs) with energy up to $>10^{20}$ eV (e.g., Waxman 1995; Vietri 1995; Waxman & Bahcall 2000; Dai & Lu 2001; Dermer 2002; Murase et al. 2006), given the hypothesis that the fireball composition is proton dominated and the protons are accelerated in the dissipative fireballs. The proton interactions with the fireball photons will produce a burst of neutrinos with energies of $\sim$PeV (e.g., Waxman & Bahcall 1997; Guetta et al. 2004; Dermer & Atoyan 2006), so detecting these neutrinos would prove the presence of the cosmic ray protons in the fireball. Despite the fact that much progress in the study of the GRBs and their afterglow has been made recently, the composition of the jet—whether it is proton–electron dominated or Poynting-flux dominated—is largely unknown. Both the baryon-dominated fireball shock model (e.g., Rees & Meszaros 1994; Paczynski & Xu 1994) and the magnetic dissipation model (e.g., Narayan & Kumar 2009; Zhang & Yan 2011) have been proposed for the central engine of the GRBs. In the magnetically dominated outflow model for the GRBs, the nonthermal proton energy fraction may be low (but see Giannios 2010), while, in the baryon-dominated outflow model, it is natural to expect proton acceleration via the shock dissipation of the kinetic energy. Since the flux of the neutrinos depends on the energy fraction of the protons in the fireball for a given burst energy, the flux or limit of the neutrino emission could constrain the proton energy fraction and, in principal, provide a useful probe for the jet composition. The proton energy fraction is also crucial in understanding whether the GRBs could provide sufficient flux for the UHECRs.

The kilometer-scale IceCube detector is the most sensitive neutrino telescope in operation, although no positive neutrino signal has been detected so far (Abbasi et al. 2010, 2011a; The IceCube Collaboration 2011). Using the 22-, 40-, and 59-string configurations, the IceCube operations all yield negative results, which have put more and more stringent constraints on the neutrino emission from the GRBs. The analysis was performed for both the point-source search from the individual GRBs and the diffuse emission from the aggregated GRBs (Abbasi et al. 2011b). According to the IceCube Collaboration (ICC), with a 40-string configuration operation between 2008 and 2009, IceCube reaches a sensitivity at the level of the expected flux from the GRBs, and the upper limit of the combined analysis of the IceCube 40- and 59-strings is 0.22 times the expected flux (Abbasi et al. 2011a). Based on this, the ICC argued that the UHECR-GRB connection is challenged (Abbasi et al. 2011a).

The calculation by the ICC is based on the formula in the Appendix of the paper of Abbasi et al. (2010) and the benchmark parameters for the internal shock model of the GRBs. However, as was also pointed out by Li (2012) and Hümmer et al. (2011), we will show that the normalization procedure used by the ICC overestimates the neutrino flux. In calculating the photon number density, the ICC also approximates the energy of all the photons by the break energy of the photon spectrum, which originates from the assumption in Guetta et al. (2004). To achieve a more accurate estimate of the expected neutrino flux, we first present a refined analytic calculation in Section 2.1,

revising the above approximations, and perform a numerical calculation in Section 2.2, taking into account the three main energy loss channels for the protons interacting with the burst photons. In Section 3, we study the effects of nonbenchmark parameters on the neutrino emission, such as the dissipation radius and the bulk Lorentz factor of the fireball. In Section 4, we calculate the accumulative diffuse neutrino emission from the GRBs and confront it with the IceCube limit on diffuse neutrinos. In Section 5, we discuss our results and provide a conclusion.

2. GRB NEUTRINO SPECTRA

Based on the assumption that protons and electrons are accelerated in the same region of a GRB, protons that interact with the photons emitted by the electron synchrotron emission or the inverse-Compton emission predominantly produce the charged and neutral pions. The charged pion subsequently decays to produce the four final-state leptons via the processes $\pi^{\pm} \rightarrow \nu_\mu(\bar{\nu}_\mu)\mu^{\pm} \rightarrow \nu_\mu(\bar{\nu}_\mu)e^{+}(e^{-})\nu_e(\bar{\nu}_e)\bar{\nu}_\mu(\nu_\mu)$, which approximately share the pion energy equally. Denoting $\Re$ as the ratio between the charged pion number and the total pion number, the fraction of the proton energy lost into each lepton is $\Re/4 f_{p\gamma}$, where $f_{p\gamma}$ is the fraction of the proton energy lost into the pions. For the proton with an energy of $\epsilon_p = \gamma_p m_p c^2$, the photomeson-interaction timescale can be calculated by (Waxman & Bahcall 1997)

$$t_{p\gamma}^{-1}(\epsilon_p) = \frac{1}{\epsilon_p}\frac{d\epsilon_p}{dt} = \frac{c}{2\gamma_p^2}\int_{\tilde{\epsilon}_{\gamma,\rm th}}^{\infty} d\tilde{\epsilon}_\gamma \sigma_{p\gamma}(\tilde{\epsilon}_\gamma)\xi(\tilde{\epsilon}_\gamma)\tilde{\epsilon}_\gamma \times \int_{\tilde{\epsilon}_\gamma/2\gamma_p}^{\infty} dx x^{-2}\frac{dn_\gamma}{dx}, \quad (1)$$

where $\sigma_{p\gamma}(\tilde{\epsilon}_\gamma)$ is the cross section of the photomeson interaction for a photon with energy $\tilde{\epsilon}_\gamma$ in the proton-rest frame, $\xi(\tilde{\epsilon}_\gamma)$ is the inelasticity, $\tilde{\epsilon}_{\gamma,\rm th}$ is the threshold of the photon energy, and $dn_\gamma/d\epsilon_\gamma$ is the GRB photon spectrum in the fluid-rest frame (Waxman & Bahcall 1997). The fraction of the proton energy loss into the pions is

$$f_{p\gamma} = 1 - \exp(-t_{\rm dyn}/t_{p\gamma}), \quad (2)$$

where $t_{\rm dyn} = R/(\Gamma c)$ is the dynamic timescale. Just for simplicity, we use $t_{\rm dyn}$ as the interaction time. Generally speaking, proton-cooling timescales can be shorter than the dynamical timescale (see Murase & Nagataki 2006a, 2006b for details), but we do not consider such complicated effects for the purpose of testing the standard model suggested by Waxman & Bahcall (1997).

Assuming that the neutrinos produced via the photomeson interaction by protons with energy ϵ_p have a constant energy, the spectrum of the neutrinos from the decay of the secondary particles, without considering the oscillation, can be obtained by

$$\epsilon_\ell \frac{dn_\ell}{d\epsilon_\ell} d\epsilon_\ell = \frac{\Re(\epsilon_p)}{4} f_{p\gamma}(\epsilon_p)\theta_\ell(\epsilon_p)\epsilon_p \frac{dn_p}{d\epsilon_p} {\rm d}\epsilon_p, \quad (3)$$

where $dn_p/d\epsilon_p$ is the spectrum of protons and $\Re$ is the ratio between the charged pion number and the total pion number as defined above in Equation (1). The subscript ℓ represents different types of neutrinos, i.e., $\ell = \nu_\mu, \bar{\nu}_\mu, \nu_e$ for muon neutrinos ν_μ produced via the decay of pions, antimuon neutrinos $\bar{\nu}_\mu$, and electron neutrinos ν_e produced via the decay of muons. If the cooling timescale of the pions or the muons is smaller than their lifetime, then the pions or the muons may cool down before they decay. Then, the neutrino flux will be suppressed by a factor of $\zeta_\pi = 1 - \exp(-t_{\pi,\rm syn}/\tau_\pi)$, where $t_{\pi,\rm syn} = 3.3\times10^{-3}\,{\rm s}\,L_{\gamma,52}^{-1}\Gamma_{2.5}^2 R_{14}^2 \epsilon_{\pi,\rm EeV}^{-1}$ is the synchrotron-cooling timescale and $\tau_\pi = 2.6\times10^{-8}\,{\rm s}\,\gamma_\pi = 186\,{\rm s}\,\epsilon_{\pi,\rm EeV}$ is the lifetime of the pions whose energy is $\epsilon_\pi = 0.2\epsilon_p$. Here, we assume that the fraction of the electron energy and the magnetic field energy are the same, i.e., $\epsilon_e = \epsilon_B$. Similarly, the suppression due to muon cooling is $\zeta_\mu = 1 - \exp(-t_{\mu,\rm syn}/\tau_\mu)$, where $t_{\mu,\rm syn} = 1.1\times10^{-3}\,{\rm s}\,L_{\gamma,52}^{-1}\Gamma_{2.5}^2 R_{14}^2 \epsilon_{\mu,\rm EeV}^{-1}$ and $\tau_\mu = 2.1\times10^{4}\,{\rm s}\,\epsilon_{\mu,\rm EeV}$ with the muon energy $\epsilon_\mu = 0.15\epsilon_p$. The suppression factor $\theta_\ell(\epsilon_p)$ is a combination of $\zeta_\pi(\epsilon_p)$ and $\zeta_\mu(\epsilon_p)$, i.e., $\theta_{\nu_\mu}(\epsilon_p) = \zeta_\pi(\epsilon_p)$ and $\theta_{\bar{\nu}_\mu(\nu_e)}(\epsilon_p) = \zeta_\pi(\epsilon_p)\zeta_\mu(\epsilon_p)$.

Considering the neutrino oscillation effect, the spectrum of the muon neutrinos (including the antimuon neutrinos) detected on the Earth is approximated as (Nagataki et al. 2003; Particle Data Group et al. 2004; Kashti & Waxman 2005; Murase 2007; Li 2012)

$$\frac{dn_\nu}{d\epsilon_\nu} = 0.2\frac{dn_{\nu_e}}{d\epsilon_{\nu_e}} + 0.4\frac{dn_{\nu_\mu}}{d\epsilon_{\nu_\mu}} + 0.4\frac{dn_{\bar{\nu}_\mu}}{d\epsilon_{\bar{\nu}_\mu}}, \quad (4)$$

where ν_μ is produced via the decay of the secondary pions and ν_e and $\bar{\nu}_\mu$ are produced via the decay of the secondary muons. Therefore, by inserting Equation (3) into Equation (4), one can numerically calculate the total spectrum of the muon neutrinos (including the antimuon neutrinos) detected on the Earth via the following equation:

$$\epsilon_\nu \frac{dn_\nu}{d\epsilon_\nu}{\rm d}\epsilon_\nu = \frac{\Re(\epsilon_p)}{4} f_{p\gamma}(\epsilon_p)\theta_\nu(\epsilon_p)\epsilon_p \frac{dn_p}{d\epsilon_p}{\rm d}\epsilon_p, \quad (5)$$

with the factor $\theta_\nu(\epsilon_p) = 0.4\zeta_\pi(\epsilon_p) + 0.6\zeta_\pi(\epsilon_p)\zeta_\mu(\epsilon_p)$ accounting for the neutrino oscillation and the cooling of the secondary particles.

The GRB photon distribution can be described by

$$\frac{dn_\gamma}{d\epsilon_\gamma} = A_\gamma\left(\frac{\epsilon_\gamma}{\epsilon_{\gamma b}}\right)^{-q}, \quad (6)$$

where $\epsilon_{\gamma,b}$ is the break energy (in the fluid-rest frame) of the photon spectrum, $q = \alpha$ for $\epsilon_\gamma < \epsilon_{\gamma b}$, and $q = \beta$ for $\epsilon_\gamma > \epsilon_{\gamma b}$. The normalized coefficient is $A_\gamma = U_\gamma[\int_{\epsilon_{\gamma,\rm min}}^{\epsilon_{\gamma,\rm max}} \epsilon_\gamma(\epsilon_\gamma/\epsilon_{\gamma b})^{-q} d\epsilon_\gamma]^{-1} = (U_\gamma/y_1\epsilon_{\gamma b}^2)$, where the energy density of the photons is $U_\gamma = L_\gamma/4\pi R^2\Gamma^2 c$, and

$$y_1 = \frac{1}{\alpha-2}\left(\frac{\epsilon_{\gamma b}}{\epsilon_{\gamma,\rm min}}\right)^{\alpha-2} - \frac{1}{\beta-2}\left(\frac{\epsilon_{\gamma b}}{\epsilon_{\gamma,\rm max}}\right)^{\beta-2} - \frac{1}{\alpha-2} + \frac{1}{\beta-2} \quad (7)$$

for $\beta \neq 2$, where $\epsilon_{\gamma,\rm min}$ and $\epsilon_{\gamma,\rm max}$ are the minimum and maximum energies of the photons, respectively. For $\beta = 2$, $y_1 = (1-(\epsilon_{\gamma,\rm min}/\epsilon_{\gamma b})^{-\alpha+2})/(-\alpha+2) + \ln(\epsilon_{\gamma,\rm max}/\epsilon_{\gamma b})$. Hereafter, we adopt the assumptions that $\epsilon_{\gamma,\rm min} = 1\,{\rm keV}$ and $\epsilon_{\gamma,\rm max} = 10\,{\rm MeV}$, just as the ICC did (Abbasi et al. 2010). If we know the redshift of the bursts, then the correction should be properly taken into account when estimating the luminosity.

The proton number per each energy interval can be described by $dn_p/d\epsilon_p = N_p\epsilon_p^{-s}$, with s being the power-law index and

N_p being the normalized coefficient. The normalized coefficient of the injected proton spectrum can be calculated by $N_p = E_p/\int_{\epsilon_{p,\min}}^{\epsilon_{p,\max}} d\epsilon_p \epsilon_p^{1-s} = E_p/\ln\epsilon_{p,\max}/\epsilon_{p,\min}$ (hereafter we set $s = 2$, as predicted by the shock acceleration theory), with E_p being the total energy in the protons and $\epsilon_{\rm p,min}$ and $\epsilon_{\rm p,max}$ being the minimum and maximum energies of the accelerated protons, respectively. We introduce the factor η_p, which denotes the ratio of the energy in the accelerated protons to the radiation energy, then the total proton energy E_p is (Murase & Nagataki 2006a)

$$E_p = \eta_p E_{\rm iso}, \tag{8}$$

where $E_{\rm iso}$ is the isotropic energy of the burst, which is obtained from the observed fluence $F_\gamma^{\rm ob}$ in the energy band of 1 keV–10 MeV and the redshift of the burst. According to Waxman (1995) and Li (2012), for mildly relativistic GRB internal shocks, we assume that the minimum proton energy is $\epsilon_{p,\min}^{\rm ob} \simeq \Gamma m_p c^2 = 3.0\times10^{11}\Gamma_{2.5}/(1+z)\,{\rm eV}$,[5] and the maximum proton energy due to the synchrotron cooling is $\epsilon_{p,\max}^{\rm ob} = 4.0\times10^{20}\Gamma_{2.5}^{3/2}R_{14}^{1/2}\epsilon_e^{1/4}\epsilon_B^{-1/4}g_1^{-1/2}L_{\gamma,52}^{-1/4}/(1+z)\,{\rm eV}$, with $g_1 \gtrsim 1$ as a factor that accounts for the uncertainty in the particle acceleration time.

2.1. Analytical Calculation

2.1.1. Neutrino Spectrum in the General Dissipation Scenario

In this subsection, we treat the dissipation radius as a free parameter, since the exact dissipation mechanism of the GRBs is not established. There are suggestions that, besides the standard internal shock model, the prompt emission arises from the dissipative photosphere or it arises at much larger radii where the magnetic-dominated outflow is dissipated through magnetic dissipation processes, such as reconnection (e.g., Narayan & Kumar 2009; Kumar & Narayan 2009; Zhang & Yan 2011).

For the analytical calculation, we adopt the Δ resonance approximation as was used in Waxman & Bahcall (1997) and Guetta et al. (2004), where the cross section peaks at the photon energy $\tilde{\epsilon}_\gamma \sim \epsilon_{\rm peak} = 0.3\,{\rm GeV}$ in the proton-rest frame. If $t_{\rm dyn} < t_{p\gamma}$, then the conversion fraction is approximated as $f_{p\gamma} \simeq t_{\rm dyn}/t_{p\gamma} = R/(\Gamma c t_{p\gamma})$. After adopting the Δ resonance approximation (Waxman & Bahcall 1997), the fraction of the proton energy converted into the pion is

$$f_{p\gamma}\left(\epsilon_p^{\rm ob}\right) \simeq \frac{0.11}{y_1}\left(\frac{2}{\alpha+1}\right)\left(\frac{1}{1+z}\right)\frac{L_{\gamma52}}{\epsilon_{\gamma b,\rm MeV}^{\rm ob}\Gamma_{2.5}^2 R_{14}} \times \begin{cases} k_1\left(\frac{\epsilon_p^{\rm ob}}{\epsilon_{p,b}^{\rm ob}}\right)^{\beta-1}, & \epsilon_p^{\rm ob} \leqslant \epsilon_{p,b}^{\rm ob} \\ \left(\frac{\epsilon_p^{\rm ob}}{\epsilon_{p,b}^{\rm ob}}\right)^{\alpha-1} + k_p, & \epsilon_p^{\rm ob} > \epsilon_{p,b}^{\rm ob}, \end{cases} \tag{9}$$

where

$$\epsilon_{p,b}^{\rm ob} = \Gamma_{\rm p}^{\rm ob} m_p c^2 = \frac{\Gamma^2 \xi_{\rm peak}}{2(1+z)^2\epsilon_{\gamma b}^{\rm ob}}, \tag{10}$$

$k_1 = \alpha + 1/\beta + 1$, and $k_p = \alpha - \beta/\beta + 1(\epsilon_p^{\rm ob}/\epsilon_{p,b}^{\rm ob})^{-2}$.[6] Note that the above approximation is valid when the radius is not too small, i.e., $R > 1.1\times10^{13}(1/y_1)(2/\alpha+1)(1/1+z)\,L_{\gamma,52}\epsilon_{\gamma b,\rm MeV}^{\rm ob,-1}\Gamma_{2.5}^{-2}\,{\rm cm}$.

Using $\epsilon_\nu = 0.05\epsilon_p$ for the Δ resonance approximation from Equation (10), we can obtain the break energy of the neutrino spectrum that corresponds to the photon spectral break:

$$\epsilon_{\nu,b}^{\rm ob} = 7.5\times10^5\,{\rm GeV}(1+z)^{-2}\Gamma_{2.5}^2\epsilon_{\gamma,\rm MeV}^{\rm ob,-1}. \tag{11}$$

The cutoff energy of the muon-neutrino spectrum due to the pion cooling can be obtained by setting $t_{\pi,\rm syn} = \tau_\pi$,

$$\epsilon_{\nu_\mu,\rm c}^{\rm ob} = \frac{3.3\times10^8}{(1+z)}L_{\gamma,52}^{-1/2}\Gamma_{2.5}^2 R_{14}\,{\rm GeV}. \tag{12}$$

For the antimuon neutrinos (and electron neutrinos) produced via the decay of the muons, an extra break is caused by the muon cooling, which is

$$\epsilon_{\lambda,\rm c}^{\rm ob} = \frac{2.4\times10^7}{(1+z)}L_{\gamma,52}^{-1/2}\Gamma_{2.5}^2 R_{14}\,{\rm GeV}, \tag{13}$$

where the subscript λ represents either the antimuon neutrino $\bar{\nu}_\mu$ or the electron neutrino ν_e.

Using Equations (3) and (9) and assuming that the fraction of the amount of the charged pions is $\Re = 1/2$, we obtain the spectrum of the muon neutrinos produced by the pion decay,

$$\left(\epsilon_{\nu_\mu}^{\rm ob}\right)^2\frac{dn_{\nu_\mu}}{d\epsilon_{\nu_\mu}^{\rm ob}} = \frac{0.014}{y_1}\left(\frac{2}{\alpha+1}\right)\left(\frac{1}{1+z}\right) \times \frac{\eta_p F_\gamma^{\rm ob}}{\ln\left(\frac{\epsilon_{\rm p,max}^{\rm ob}}{\epsilon_{\rm p,min}^{\rm ob}}\right)}\frac{L_{\gamma,52}}{\epsilon_{\gamma b,\rm MeV}^{\rm ob}\Gamma_{2.5}^2 R_{14}} \times \begin{cases} \left(\frac{\epsilon_{\nu_\mu}^{\rm ob}}{\epsilon_{\nu,b}^{\rm ob}}\right)^{\beta-1}, & \epsilon_{\nu_\mu}^{\rm ob} \leqslant \epsilon_{\nu,b}^{\rm ob} \\ \left(\frac{\epsilon_{\nu_\mu}^{\rm ob}}{\epsilon_{\nu,b}^{\rm ob}}\right)^{\alpha-1}, & \epsilon_{\nu,b}^{\rm ob} < \epsilon_{\nu_\mu}^{\rm ob} \leqslant \epsilon_{\nu_\mu,\rm c}^{\rm ob} \\ \left(\frac{\epsilon_{\nu_\mu}^{\rm ob}}{\epsilon_{\nu,b}^{\rm ob}}\right)^{\alpha-1}\left(\frac{\epsilon_{\nu_\mu}^{\rm ob}}{\epsilon_{\nu_\mu,\rm c}^{\rm ob}}\right)^{-2}. & \epsilon_{\nu_\mu}^{\rm ob} > \epsilon_{\nu_\mu,\rm c}^{\rm ob}. \end{cases} \tag{14}$$

Similarly, the spectrum of the antimuon (and electron) neutrinos produced by the muon decay is approximated by

$$\left(\epsilon_\lambda^{\rm ob}\right)^2\frac{dn_\lambda}{d\epsilon_\lambda^{\rm ob}} = \frac{0.014}{y_1}\left(\frac{2}{\alpha+1}\right)\left(\frac{1}{1+z}\right) \times \frac{\eta_p F_\gamma^{\rm ob}}{\ln\left(\frac{\epsilon_{\rm p,max}^{\rm ob}}{\epsilon_{\rm p,min}^{\rm ob}}\right)}\frac{L_{\gamma52}}{\epsilon_{\gamma b,\rm MeV}^{\rm ob}\Gamma_{2.5}^2 R_{14}} \times \begin{cases} \left(\frac{\epsilon_\lambda^{\rm ob}}{\epsilon_{\nu,b}^{\rm ob}}\right)^{\beta-1}, & \epsilon_\lambda^{\rm ob} \leqslant \epsilon_{\nu,b}^{\rm ob} \\ \left(\frac{\epsilon_\lambda^{\rm ob}}{\epsilon_{\nu,b}^{\rm ob}}\right)^{\alpha-1}, & \epsilon_{\nu,b}^{\rm ob} < \epsilon_\lambda^{ob} \leqslant \epsilon_{\lambda,\rm c}^{\rm ob} \\ \left(\frac{\epsilon_\lambda^{\rm ob}}{\epsilon_{\nu,b}^{\rm ob}}\right)^{\alpha-1}\left(\frac{\epsilon_\lambda^{ob}}{\epsilon_{\lambda,\rm c}^{ob}}\right)^{-2}, & \epsilon_{\lambda,\rm c}^{\rm ob} < \epsilon_\lambda^{ob} < \epsilon_{\nu_\mu,\rm c}^{\rm ob} \\ \left(\frac{\epsilon_\lambda^{\rm ob}}{\epsilon_{\nu,b}^{\rm ob}}\right)^{\alpha-1}\left(\frac{\epsilon_\lambda^{\rm ob}}{\epsilon_{\lambda,\rm c}^{ob}}\right)^{-2}\left(\frac{\epsilon_\lambda^{\rm ob}}{\epsilon_{\nu_\mu,\rm c}^{ob}}\right)^{-2}, & \epsilon_{\nu_\mu,\rm c}^{\rm ob} < \epsilon_\lambda^{ob}. \end{cases} \tag{15}$$

Then, one can obtain the $\nu_\mu + \bar{\nu}_\mu$ spectrum after considering the neutrino oscillation effect by substituting Equations (14) and (15) into Equation (4).

[5] In some other papers, $\epsilon_{p,\min}^{\rm ob} \simeq 4\Gamma m_p c^2$ or $\epsilon_{p,\min}^{\rm ob} \simeq 10\Gamma m_p c^2$ is adopted because the relative Lorentz factor is of the order of 1–10, where the higher values favor the efficiency internal shocks.

[6] Hereafter, we abandon the coefficients k_1 and k_ℓ for brevity in the following equations, since $k_1 \simeq 1$ and $k_\ell \simeq 0$, where $k_\ell = \alpha - \beta/\beta + 1(\epsilon_\ell^{\rm ob}/\epsilon_{\ell,b}^{\rm ob})^{-2}$ and ℓ represents the three types of neutrinos, i.e., electron neutrinos and muon(antimuon) neutrinos. However, we still adopt that in our analytic calculations.

2.1.2. Neutrino Spectrum in the Internal Shock Scenario

In this subsection, we assume the standard internal shock scenario with a dissipation radius at $R = 2\Gamma^2 ct_v^{\rm ob}/(1+z)$, where $t_v^{\rm ob}$ is the observed variability timescale of the GRB emission. The conversion fraction $f_{p\gamma}$ is given by

$$f_{p\gamma}\left(\epsilon_p^{\rm ob}\right) \simeq \frac{0.18}{y_1}\left(\frac{2}{\alpha+1}\right)\frac{L_{\gamma 52}}{\epsilon_{\gamma b,{\rm MeV}}^{\rm ob}\Gamma_{2.5}^4 t_{v,-2}^{\rm ob}} \times \begin{cases} \left(\frac{\epsilon_p^{\rm ob}}{\epsilon_{p,b}^{\rm ob}}\right)^{\beta-1}, & \epsilon_p \leqslant \epsilon_{p,b}^{\rm ob} \\ \left(\frac{\epsilon_p^{\rm ob}}{\epsilon_{p,b}^{\rm ob}}\right)^{\alpha-1}, & \epsilon_p > \epsilon_{p,b}^{\rm ob}. \end{cases} \quad (16)$$

Then, the spectrum of the muon neutrinos produced via the pion decay is approximated by

$$\left(\epsilon_{\nu_\mu}^{\rm ob}\right)^2\frac{dn_{\nu_\mu}}{d\epsilon_{\nu_\mu}^{\rm ob}} = \frac{0.023}{y_1}\left(\frac{2}{\alpha+1}\right)\frac{\eta_p F_\gamma^{\rm ob}}{\ln\left(\frac{\epsilon_{p,\rm max}^{\rm ob}}{\epsilon_{p,\rm min}^{\rm ob}}\right)}\frac{L_{\gamma,52}}{\epsilon_{\gamma b,{\rm MeV}}^{\rm ob}\Gamma_{2.5}^4 t_{v,-2}^{\rm ob}} \times \begin{cases} \left(\frac{\epsilon_{\nu_\mu}^{\rm ob}}{\epsilon_{\nu,b}^{\rm ob}}\right)^{\beta-1}, & \epsilon_{\nu_\mu}^{\rm ob} \leqslant \epsilon_{\nu,b}^{\rm ob} \\ \left(\frac{\epsilon_{\nu_\mu}^{\rm ob}}{\epsilon_{\nu,b}^{\rm ob}}\right)^{\alpha-1}, & \epsilon_{\nu,b}^{\rm ob} < \epsilon_{\nu_\mu}^{\rm ob} \leqslant \epsilon_{\nu_\mu,{\rm c}}^{\rm ob}, \\ \left(\frac{\epsilon_{\nu_\mu}^{\rm ob}}{\epsilon_{\nu,b}^{\rm ob}}\right)^{\alpha-1}\left(\frac{\epsilon_{\nu_\mu}^{\rm ob}}{\epsilon_{\nu_\mu,{\rm c}}^{\rm ob}}\right)^{-2}, & \epsilon_{\nu_\mu}^{\rm ob} > \epsilon_{\nu_\mu,{\rm c}}^{\rm ob} \end{cases} \quad (17)$$

and the spectrum of the antimuon (electron) neutrinos produced via the muon decay is approximated by

$$\left(\epsilon_\lambda^{\rm ob}\right)^2\frac{dn_\lambda}{d\epsilon_\lambda^{\rm ob}} = \frac{0.023}{y_1}\left(\frac{2}{\alpha+1}\right)\frac{\eta_p F_\gamma^{\rm ob}}{\ln\left(\frac{\epsilon_{p,\rm max}^{\rm ob}}{\epsilon_{p,\rm min}^{\rm ob}}\right)}\frac{L_{\gamma,52}}{\epsilon_{\gamma b,{\rm MeV}}^{\rm ob}\Gamma_{2.5}^4 t_{v,-2}^{\rm ob}} \times \begin{cases} \left(\frac{\epsilon_\lambda^{\rm ob}}{\epsilon_{\nu,b}^{\rm ob}}\right)^{\beta-1}, & \epsilon_\lambda^{\rm ob} \leqslant \epsilon_{\nu,b}^{\rm ob} \\ \left(\frac{\epsilon_\lambda^{\rm ob}}{\epsilon_{\nu,b}^{\rm ob}}\right)^{\alpha-1}, & \epsilon_{\nu,{\rm b}}^{\rm ob} < \epsilon_\lambda^{\rm ob} \leqslant \epsilon_{\lambda,{\rm c}}^{\rm ob} \\ \left(\frac{\epsilon_\lambda^{\rm ob}}{\epsilon_{\nu,b}^{\rm ob}}\right)^{\alpha-1}\left(\frac{\epsilon_\lambda^{\rm ob}}{\epsilon_{\lambda,{\rm c}}^{\rm ob}}\right)^{-2}, & \epsilon_{\lambda,{\rm c}}^{\rm ob} < \epsilon_\lambda^{\rm ob} < \epsilon_{\nu_\mu,{\rm c}}^{\rm ob} \\ \left(\frac{\epsilon_\lambda^{\rm ob}}{\epsilon_{\nu,b}^{\rm ob}}\right)^{\alpha-1}\left(\frac{\epsilon_\lambda^{\rm ob}}{\epsilon_{\lambda,{\rm c}}^{\rm ob}}\right)^{-2}\left(\frac{\epsilon_\lambda^{\rm ob}}{\epsilon_{\nu_\mu,{\rm c}}^{\rm ob}}\right)^{-2}, & \epsilon_{\nu_\mu,{\rm c}}^{\rm ob} < \epsilon_\lambda^{\rm ob}, \end{cases} \quad (18)$$

where the cutoff energies are

$$\epsilon_{\nu_\mu,{\rm c}}^{\rm ob} = \frac{2.0\times 10^8}{(1+z)^2}L_{\gamma,52}^{-1/2}\Gamma_{2.5}^4 t_{v,-2}^{\rm ob}\,{\rm GeV} \quad (19)$$

and

$$\epsilon_{\lambda,{\rm c}}^{\rm ob} = \frac{1.4\times 10^7}{(1+z)^2}L_{\gamma,52}^{-1/2}\Gamma_{2.5}^4 t_{v,-2}^{\rm ob}\,{\rm GeV}, \quad (20)$$

with λ representing the antimuon and the electron neutrinos ($\bar{\nu}_\mu$ and ν_e) produced by the muon decay, and

$$\frac{\epsilon_{p,\rm max}^{\rm ob}}{\epsilon_{p,\rm min}^{\rm ob}} = 1.0\times 10^9\Gamma_{2.5}^{3/2}\left(t_{v,-2}^{\rm ob}\right)^{1/2}L_{\gamma,52}^{-1/4}\epsilon_e^{1/4}\epsilon_B^{-1/4}g_1^{-1/2}. \quad (21)$$

By substituting Equations (17) and (18) into Equation (4), we can analytically obtain the neutrino spectrum. To illustrate the difference between our calculation and the ICC calculation, we calculate the neutrino spectrum for one typical GRB with benchmark parameters, shown in Figure 1. Compared with the ICC calculation (the dark gray solid line), our spectrum (the purple solid line) consists of more structures resulting from the sum of the contributions by the three types of neutrinos, for which the pion cooling, the muon cooling, and the oscillation effect are considered. Furthermore, the flux level predicted by our modified analytical calculation is a factor of ∼20 lower than that obtained by the ICC (Abbasi et al. 2010, 2011a, The IceCube Collaboration 2011). This mainly arises from two differences in the calculation.

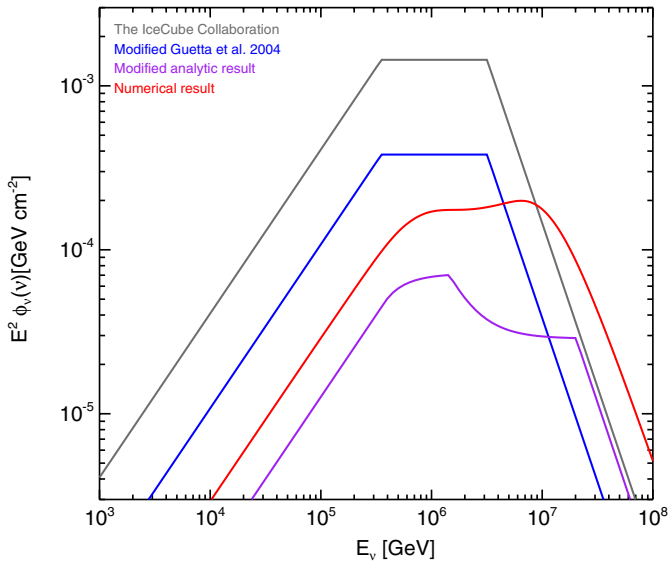

Figure 1. Neutrino spectrum for a typical GRB, using the method adopted by the ICC (Abbasi et al. 2010, 2011a; ICC 2011) (dark gray solid line), the modified Guetta et al. (2004) method (blue solid line), our modified analytical method (purple solid line), and our numerical method (red solid line). The parameters used in the calculation for this GRB are $\alpha = 1$, $\beta = 2$, fluence $F_\gamma^{\rm ob} = 10^{-5}\,{\rm erg\,cm^{-2}}$ (in 10 keV to 1 MeV), $z = 2.15$, peak energy $\epsilon_{\gamma,b}^{ob} = 200\,{\rm keV}$, peak luminosity $L_\gamma = 10^{52}\,{\rm erg\,s^{-1}}$, bulk Lorentz factor $\Gamma = 10^{2.5}$, the observed variability timescale $t_v^{\rm ob} = 0.01\,{\rm s}$, and the baryon ratio $\eta_p = 10$.

(A color version of this figure is available in the online journal.)

1. We use Equation (3), where the conversion fraction $f_{p\gamma}$ is a function of the proton energy ϵ_p as shown by Equation (16), to normalize the neutrino flux to the proton flux, which means that only a fraction of the protons can efficiently produce neutrinos. This corrects the ICC's inaccurate use of the energy-independent conversion fraction in the normalization of the neutrino flux (Li 2012; Hümmer et al. 2011; Murase et al. 2012). The calculation of Guetta et al. (2004)[7] normalized the flux based on the differential spectrum so that it does not suffer from this problem. The spectrum obtained using the calculation from Guetta et al.

[7] Guetta et al. (2004) calculated the neutrino spectrum by assuming a flat, high-energy electron spectrum (i.e., $dN_e/d\gamma_e \propto \gamma_e^{-2}$), and by using an electron equipartition fraction ϵ_e^G that represents the ratio of the nonthermal electron energy over one energy decade to the UHECR energy over one energy decade. The neutrino flux is normalized by $\epsilon_\nu^2(dN_\nu/d\epsilon_\nu) = (1/8)(1/\epsilon_e^G)(F_\gamma^{\rm ob}/\ln 10)f_\pi$ (see their Equation A19). Note that other normalization procedures are also possible, and this ϵ_e^G is typically larger than the conventional ϵ_e, which is defined as the ratio of the total nonthermal electron energy to the total internal energy (including both thermal and nonthermal protons).

(2004)[8] is shown as the blue solid line in Figure 1, and the middle of Equation (A.15) in their paper is used, assuming that the bolometric luminosity is the luminosity at the break energy. The flux is lower than the result obtained by the ICC (the dark gray solid line in Figure 1) by a factor of ∼4.

2. In calculating the photon number density, we consider the photon energy distribution according to the real photon spectrum, reflected by the normalized coefficient $A_\gamma \simeq U_\gamma / y_1 \epsilon_{\gamma b}^2$, where y_1 is shown in Equation (7). The ICC approximates the energy of all the photons using the break energy of the photon spectrum. This leads to a flux with a factor of ∼3–6 lower than the result from the ICC for typical α and β values and $\epsilon_{\gamma b} \sim 100$–1000 keV in the GRB spectrum.

Finally, we achieve a neutrino spectral flux (purple solid line) lower than the one predicted by the ICC (dark gray solid line) by a factor of ∼20 for a typical GRB, as shown in Figure 1. Of course, the suppression factor is different for the GRBs with different parameters.

2.2. Numerical Results

Besides the baryon resonance, the direct pion process, the multipion process, and the diffractive scattering also contribute to the total $p\gamma$ cross section. Therefore, in our numerical calculation, we adopt a more precise cross section for the photomeson interaction, including three main channels, i.e., the Δ resonance process, the direct pion process, and the multipion process. For simplicity, we assume that the inelasticity is $\xi = 0.2$ for $\bar{\epsilon}_\gamma < 983$ MeV and $\xi = 0.6$ for $\bar{\epsilon}_\gamma \gtrsim 983$ MeV (Atoyan & Dermer 2001). Then, by inserting the cross sections and the inelasticity into Equation (1), and using Equation (2), we can obtain the fractions of proton energy that are converted to pions. The average fractions of the charged pions are set to $\Re_\Delta = 1/3$ for the Δ resonance process, $\Re_{\rm dir} = 2/3$ for the direct-pion production, and $\Re_{\rm mul} = 2/3$ for the multipion production, based on numerical investigations (Mucke et al. 1999; Mücke et al. 2000; Murase & Nagataki 2006a, 2006b; Murase et al. 2006; Murase 2007; Baerwald et al. 2011). In addition, we assume that the neutrino energy is $\epsilon_\nu = 0.05\epsilon_p$ for the Δ-resonance and direct-pion production channels, and we assume $\epsilon_\nu = 0.03\epsilon_p$ for the multipion production channel. By inserting these quantities into Equations (1), (2), and (5), we can obtain the spectrum of the neutrino emission produced via the three dominant channels. Although this simplified numerical approach is different from more detailed, fully numerical calculations (Murase & Nagataki 2006a, 2006b; Murase 2007; Baerwald et al. 2011), it is enough for our purpose and saves calculation time.

In Figure 1, we also show this numerical result (the red solid line) for comparison. The flux obtained with this numerical calculation is about 2–3 times larger than the analytical result in the energy range 10^5 GeV–3×10^6 GeV for a typical GRB, which is consistent with Murase & Nagataki (2006a, 2006b) and Baerwald et al. (2011). So, the analytic calculation presented in the above section can still be used as a rough approximation.

2.3. Confronting the Calculations with the IC59+40 Observations

A total of 215 GRBs are observed during the operations in the 40-string and 59-string configurations of IceCube and they yield negative results. In this section, we calculate the neutrino flux for the same 215 GRBs using the same burst parameters as the ICC. The information for these samples was taken from the Web site grbweb.icecube.wisc.edu[9] and the Gamma-ray Coordinates Network (GCN). For the unmeasured parameters, we adopt the same average values used in Abbasi et al. (2010, 2011a). We assume that the ratio of proton energy to radiation energy is $\eta_p = 10$, which is equivalent to $1/f_e = 10$ in the ICC calculation. We adopt the internal-shock model with a shock radius at $R = 2\Gamma^2 c t_v^{\rm ob}/(1+z)$, where the Lorentz factor is $\Gamma = 10^{2.5}$ and the observed variability timescale is $t_v^{\rm ob} = 0.01$ s for each of the long GRBs and $t_v^{\rm ob} = 0.001$ s for each of the short GRBs, just as the ICC did. The diffuse neutrino flux can be obtained by the total neutrino fluence for 215 individual GRBs multiplied by a factor of 7.83×10^{-9} sr^{-1} s^{-1}, assuming that 667 uniform GRBs are generated per year. By adopting the effective area of IC59 and IC40 as a function of the zenith angle, we can calculate the expected number of neutrinos with an energy from 10^5 GeV to 3×10^6 GeV (Abbasi et al. 2010, 2011a). The corresponding combined 90% confidence level (CL) upper-limit spectrum can be obtained by assuming that the limited amount of neutrino events is $n_{\rm lim} \simeq 1.9$ in the energy range of 10^5 GeV to 3×10^6 GeV as in the ICC (2011).

In Figure 2, we show the 215 neutrino spectra (light red thin solid lines) for the individual GRBs. The sum of these is presented as the thick red solid line, which is about a factor of ∼10 lower than that predicted by the ICC (the dark gray solid line). As can be seen, the neutrinos predicted by the ICC and the modified method in Guetta et al. (2004) (dark gray solid line and blue solid line, respectively) are above the 90% CL upper limits (dark gray dashed line and blue dashed line) for the combined IC40 and IC59 data analysis, while our predicted neutrino flux is below the corresponding upper limit (the red dashed line). We find that the total expected number of neutrinos with an energy from 10^5 GeV to 3×10^6 GeV is 0.74, which is 36% of the 90% CL upper limit.

3. CONSTRAINTS ON THE FIREBALL PROPERTIES

3.1. Uncertainty in the Dissipation Radius

In Section 2.1.1, we do not assume a specific dissipation model for the GRB emission, but we leave the dissipation radius as a free parameter. Internal shocks occur across a wide parameter range (e.g., Nakar & Piran 2002), and even larger radii are suggested in some other dissipation models (e.g., Narayan & Kumar 2009; Zhang & Yan 2011). In Figure 3, we show the total neutrino spectra for 215 GRBs by assuming some fixed dissipation radii for every GRB in the range $R =$

[8] In our paper, we used the nonthermal baryon-loading parameter η_p, defined as the ratio between the total energy in accelerating protons and the total radiation energy at observed bands, to normalize the neutrino flux through $\epsilon_\nu^2 (dN_\nu/d\epsilon_\nu) = (1/8)(\eta_p/\ln(\epsilon_{p,\rm max}/\epsilon_{p,\rm min}))F_\gamma^{\rm ob} f_{p\gamma}$. The lines of "modified Guetta et al. (2004)" in Figures 1 and 2 are obtained by using the benchmark value of $\eta_p = 10$, which corresponds to $\epsilon_e^G = \ln(\epsilon_{p,\rm max}/\epsilon_{p,\rm min})/\ln(10)(1/\eta_p) \sim 1$ in Equation (A19) in Guetta et al. (2004). Choosing $\epsilon_e^G = 0.1$ in Guetta et al. (2004) would correspond to a higher baryon loading factor of $\eta_p = \ln(\epsilon_{p,\rm max}/\epsilon_{p,\rm min})/\ln(10)(1/\epsilon_e^G) \sim 100$ in our paper. Note that the GRB-UHECR hypothesis might suggest such high loading factors if the local GRB rate is 0.01–0.1 Gpc^{-3} yr^{-1} or the local luminosity density is sufficiently smaller than $\sim 10^4$4 erg Mpc^{-3} yr^{-1}, and those relatively optimistic cases are constrained by IceCube under reasonable assumptions, as expected by Murase & Nagataki (2006b).

[9] When information from this Web site contradicts or is different from that given by the GCN, we use the information from the GCN.

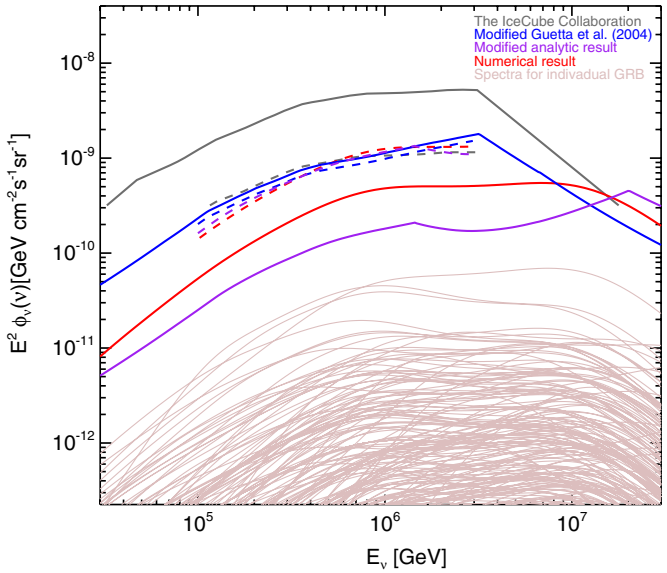

Figure 2. Neutrino spectra numerically calculated by adopting the internal shock radius $R = 2\Gamma^2 ct_v^{ob}/(1+z)$ for 215 GRBs (light red lines) observed during the IceCube operations in the 40-string and 59-string configurations. We use the same GRB samples, the same assumptions for the GRB parameters, and the same effective area as a function of the zenith angle as those used by the ICC. The thick red solid line represents the sum of the neutrino spectra of the 215 GRBs and the thick red dashed line is the corresponding 90% CL upper limit of IceCube. The thick dark gray solid line and dashed line are the predicted total neutrino spectrum and the corresponding 90% CL upper limit given by the ICC for the combined data analysis of IC40 and IC59, respectively. The blue solid and dashed lines correspond to the expected spectra and the 90% CL upper limit obtained by using the modified method in Guetta et al. (2004). The purple lines represent our modified analytical calculation as a comparison. For the above calculations, we adopt benchmark parameters, such as the peak luminosity $L_\gamma = 10^{52}$ erg s^{-1}, the observed variability timescale $t_v^{ob} = 0.01$ s for the long GRBs, the Lorentz factor $\Gamma = 10^{2.5}$, and the baryon ratio $\eta_p = 10$ for every GRB.

(A color version of this figure is available in the online journal.)

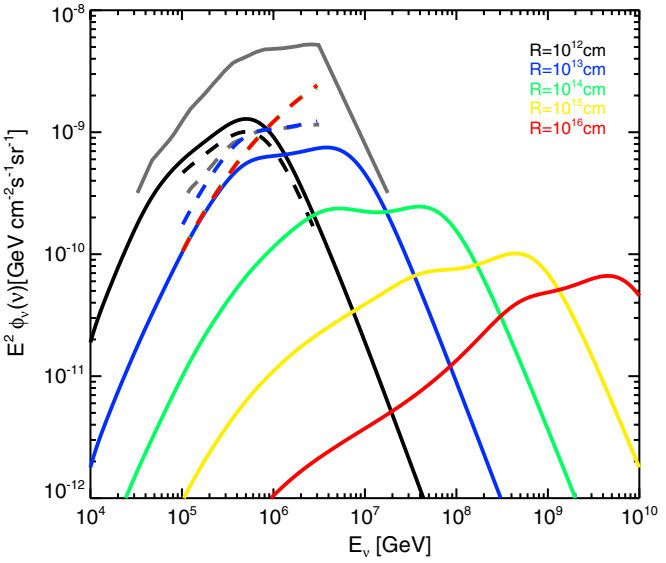

Figure 3. Spectra of the total neutrino emission produced by 215 GRBs, assuming the same dissipation radius for every GRB at $R = 10^{12}$ cm (the black solid line), $R = 10^{13}$ cm (the blue solid line), $R = 10^{14}$ cm (the green solid line), $R = 10^{15}$ cm (the yellow solid line), and $R = 10^{16}$ cm (the red solid line). The corresponding upper limits are shown by the dashed lines. Other parameters are the same as those used in Figure 2. Note that the red, green, and yellow dashed lines overlap with each other because the spectrum shape of the red, green, and yellow solid lines is similar in the energy range of 10^5 GeV–3×10^6 GeV.

(A color version of this figure is available in the online journal.)

10^{12}–10^{16} cm.[10] The figure shows that the neutrino flux for the case of $R = 10^{12}$ cm (the black solid line) would exceed the corresponding IceCube upper limit (the black dashed line) as long as the baryon-loading factor is sufficiently greater than unity. If we fix $\eta_p = 10$, then the nondetection requires that the dissipation radius be larger than 4×10^{12} cm. We note that, when the emission radius is too small, the maximum energy of the accelerating particles is limited due to the strong photohadronic and/or radiation cooling, and the neutrino emission can be more complicated due to the strong pion/muon cooling, so a more careful study is needed to obtain quantitative constraints on η_p in this regime. On the other hand, the larger dissipation radius leads to a lower neutrino flux and higher cooling break energy according to Equations (12) and (13). The shift of the first break to higher energies for larger dissipation radii is due to those GRBs with $\alpha > 1$, whose neutrino spectral peaks located at the cooling breaks dominantly contribute to the neutrino flux.

3.2. Uncertainty in the Bulk Lorentz Factor

In the previous subsections, we took either the variability or the dissipation radius as a principal parameter, given a Lorentz factor, i.e., $\Gamma = 10^{2.5}$. For those bursts without a measured redshift, we took $L_\gamma = 10^{52}$ erg s^{-1} for the peak luminosity, as was done by the ICC. However, it was found recently that the bulk Lorentz factor could significantly vary among the bursts, and there is an inherent relation between the Lorentz factor and the isotropic energy or the peak luminosity (Liang et al. 2010; Ghirlanda et al. 2012). As shown by Equations (17) and (18), the neutrino flux is very sensitive to the bulk Lorentz factor, so we can use the inherent relation to obtain more realistic values for the Lorentz factors and, hence, a more reliable estimate of the neutrino flux.

By identifying the onset time of the forward shock from the optical afterglow observations, Liang et al. (2010) and Lv et al. (2011) obtain the bulk Lorentz factors for a sample of GRBs. They furthermore found a correlation between the bulk Lorentz factor and the isotropic energy of the burst, given by[11]

$$\Gamma_L = 118 E_{\rm iso,52}^{0.26}. \quad (22)$$

Ghirlanda et al. (2012) revisit this problem with a large sample and obtain a relation as

$$\Gamma_G = 29.8 E_{\rm iso,52}^{0.51}. \quad (23)$$

Compared with the benchmark model, which assumes $\Gamma = 10^{2.5}$ for all of the bursts, the value of Γ obtained from these relations is lower for the bursts with the isotropic energy $E_{\rm iso} \lesssim (4.4\text{–}9.4) \times 10^{53}$ erg.

Ghirlanda et al. (2012) also obtained the relation between the bulk Lorentz factor and the peak luminosity, i.e.,

$$\Gamma_{G_L} = 72.1 L_{\gamma,52}^{0.49}. \quad (24)$$

[10] If the radius is smaller than the photosphere radius, then the neutrino emission produced by the $p - p$ interactions becomes important (Wang & Dai 2009; Murase 2008); this scenario is not considered here.

[11] We adopt only the center value for the relationships presented hereafter.

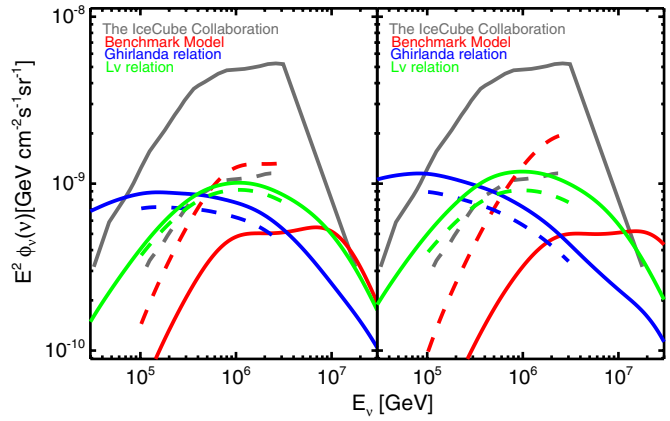

Figure 4. Spectra of the total neutrino emission produced by 215 GRBs, assuming different fireball parameters in the standard internal shock model. The solid red line represents the spectrum that adopts the same benchmark parameters seen in Figure 2. The solid blue line represents the spectrum that adopts the relations of $E_{\rm iso}-\Gamma$ and $\epsilon_{\gamma b}^{\rm ob}-L_\gamma$ in Ghirlanda et al. (2012). The solid green line represents the spectrum that adopts the relation of $E_{\rm iso}-\Gamma$ in Lv et al. (2011) and $\epsilon_{\gamma b}^{\rm ob}-L_\gamma$ in Ghirlanda et al. (2012). The dashed lines are the corresponding upper limits by IC40+IC59. Left panel: $z=2.15$ is assumed for the long GRBs without the measured redshifts. Right panel: $z=1$ is assumed for the long GRBs without the measured redshifts.

(A color version of this figure is available in the online journal.)

The value of Γ obtained from this relation is lower than $10^{2.5}$ for the bursts with luminosity of $L_p<2.0\times10^{53}\,{\rm erg\,s^{-1}}$.

Yonetoku et al. (2004) and Ghirlanda et al. (2012) found an inherent relation between the peak energy of the photon spectrum and the peak luminosity. Therefore, one can obtain the peak luminosity from the observed break energy of the photon spectrum $\epsilon_{\gamma,b}^{\rm ob}$ and the redshift z by adopting the $\epsilon_{\gamma,b}^{\rm ob}-L_\gamma$ relation, which is

$$L_{\gamma G,52}=7.54\left[\epsilon_{\gamma b,{\rm MeV}}^{\rm ob}(1+z)\right]^{1.75}, \quad (25)$$

derived by Ghirlanda et al. (2012).

We use the above inherent relations to calculate both the Lorentz factor Γ and the peak luminosity L_γ, and then we calculate the neutrino flux produced by the same 215 GRBs, shown in Figure 4. The main differences in the neutrino spectrum resulted from the use of different choices for the value of the bulk Lorentz factor, and these differences can be summarized as:

1. The peak energy of the neutrino spectrum shifts to a lower energy for the models that adopt the relations in Ghirlanda et al. (2012) and Lv et al. (2011). This is due to the fact that, for the majority of the 215 GRBs, the values of Γ derived with these inherent relations are lower than the benchmark value of $10^{2.5}$, which leads to a lower peak energy in the neutrino spectrum according to Equation (11). Also, the cutoff energy shifts to lower energies for these models according to Equations (19) and (20).
2. The peak flux of the neutrino spectrum increases for the two models that adopt the inherent relations. This is due to the fact that a lower Lorentz factor leads to a higher neutrino production efficiency in the internal shock model. The predicted neutrino flux for both models adopting $E_{\rm iso}-\Gamma$ relations in Ghirlanda et al. (2012) and Lv et al. (2011) exceeds the IceCube upper limit, which implies that the baryon ratio of $\eta_p\lesssim10$ if $t_{\rm v}^{\rm ob}=0.01$ s for long GRBs is correct.

Table 1
Critical Value of the Baryon Ratio $\eta_{p,c}$ for the Combined IC40+IC59 Analysis

$L_\gamma({\rm erg\,s^{-1}})$	Γ	z	$\eta_{p,c}$
10^{52}	$10^{2.5}$	2.15	26.0
		1	39.9
$L_{\gamma\rm G}$	$\Gamma_{\rm G}$	2.15	8.16
		1	7.79
$L_{\gamma\rm G}$	$\Gamma_{\rm L}$	2.15	9.07
		1	7.72

Notes. Critical value of the baryon ratio $\eta_{p,c}$ for the combined IC40+IC59 analysis obtained by adopting different assumptions for the bulk Lorentz factor, the peak luminosity, and the redshift (for the long GRBs without the measured redshifts). $L_{\gamma\rm G}$ represents the peak luminosity obtained by using the $\epsilon_{\gamma b}^{\rm ob}-L_\gamma$ relation in Ghirlanda et al. (2012). $\Gamma_{\rm G}$ and $\Gamma_{\rm L}$ are the Lorentz factors obtained with the relations of $E_{\rm iso}-\Gamma$ in Lv et al. (2011) and Ghirlanda et al. (2012), respectively. Here, the observed variability timescale for the long GRBs is assumed to be 0.01 s.

In the left panel of Figure 4, we take the redshift $z=2.15$ for those long GRBs without a measured redshift, the amount of which is about 84% of the total amount of GRBs. For the benchmark model, the neutrino flux would not be significantly affected since it is independent of the redshift according to Equations (17) and (18). However, the value of the redshift can affect the flux of the neutrino spectrum for models adopting the inherent relations. For a fixed observed fluence of the γ-ray emission, a smaller redshift will lead to a smaller peak luminosity or isotropic energy. As a result, the Lorentz factor, derived from the inherent relations, will be lower, which leads to a higher neutrino production efficiency. As shown in the right panel of Figure 4, the flux for the two models adopting inherent relations increases if we take $z=1$ for those long GRBs without measured redshifts.

In the above discussions, we have implicitly assumed that the baryon ratio of $\eta_p=10$ for the GRBs, in accordance with the notation of $f_e=0.1$ in Abbasi et al. (2010). This value comes from the assumption that the radiation efficiency for the GRBs is typically 0.1 and that most of the dissipated internal energy goes into the accelerated protons. However, the fraction of energy in the protons, and hence, the value of η_p, is not well known. The null result of the IceCube observations allows us to put some constraints on this value. We define $\eta_{p,c}$ as the critical value, above which the GRBs would be detected by the corresponding IceCube configurations. In Table 1, we list the corresponding value of $\eta_{p,c}$ for the combined IC40 and IC59 analysis. However, one should keep in mind that $\eta_{p,c}$ depends on the choice of $t_{\rm v}^{\rm ob}$, so it should be larger for larger values of $t_{\rm v}^{\rm ob}$.

4. DIFFUSE NEUTRINO EMISSION FROM GRBs

Recently, IceCube also reported observations of diffuse neutrinos by the 40-string configuration. The nondetection yields an upper limit of 8.9×10^{-9} GeV cm^{-1} s^{-1} sr^{-1} for the diffuse neutrino flux, assuming an E^{-2} neutrino spectrum (Abbasi et al. 2011b). The expected diffuse GRB neutrino flux can be obtained by summing the contributions of all the GRBs in the entire universe. To this aim, we also take into account the number distribution of the GRBs over the luminosity (i.e., the luminosity function) as well as the number distribution at the different redshifts. The luminosity affects the results when one adopts specific relations such as Equations (22), or (23), or (25).

We employ three different luminosity functions and the corresponding source density evolution functions to describe the distribution of the GRB number over the luminosity and the redshift. One luminosity function is suggested by Liang et al. (2007; hereafter LF-L),

$$\frac{dN}{dL_\gamma} = \rho_0 \Phi_0 \left[\left(\frac{L_\gamma}{L_{\gamma b}} \right)^{\alpha_1} + \left(\frac{L_\gamma}{L_{\gamma b}} \right)^{\alpha_2} \right]^{-1}, \quad (26)$$

where $\rho_0 = 1.2\,\mathrm{Gpc^{-3}\,yr^{-1}}$ is the local event rate of the GRBs and Φ_0 is a normalization constant to ensure that the integral over the luminosity function is equal to the local event rate ρ_0. This luminosity function breaks at $L_{\gamma b} = 2.25 \times 10^{52}\,\mathrm{erg\,s^{-1}}$, with indices of $\alpha_1 = 0.65$ and $\alpha_2 = 2.3$ for each segment. The normalized number distribution of the GRBs with the redshift used by Liang et al. (2007) in obtaining this luminosity function is (Porciani & Madau 2001)

$$S(z) = 23 \frac{e^{3.4z}}{e^{3.4z} + 22.0}. \quad (27)$$

Wanderman & Piran (2010) also suggested a luminosity function in the form of a broken power law (hereafter LF-W):

$$\frac{dN}{dL_\gamma} = \rho_0 \Phi_0 \begin{cases} \left(\frac{L_\gamma}{L_{\gamma b}} \right)^{-\alpha_1} & L < L_{\gamma b}, \\ \left(\frac{L_\gamma}{L_{\gamma b}} \right)^{-\alpha_2} & L \geqslant L_{\gamma b}, \end{cases} \quad (28)$$

where $\rho_0 = 1.3\ \mathrm{Gpc^{-3}\,yr^{-1}}$, $\alpha_1 = 1.2$, $\alpha_2 = 2.4$, and the break luminosity $L_{\gamma b} = 10^{52.5}\,\mathrm{erg\,s^{-1}}$. The corresponding normalized number distribution with the redshift is described by

$$S(z) = \begin{cases} (1+z)^{2.1} & z < 3, \\ (1+z)^{-1.4} & z \geqslant 3. \end{cases} \quad (29)$$

Another luminosity function we consider here is suggested by Guetta & Piran (2007; hereafter LF-G), which is in the same form as that of Wanderman & Piran (2010) but with different parameters, i.e., $\rho_0 = 0.27\,\mathrm{Gpc^{-3}\,yr^{-1}}$, $\alpha_1 = -1.1$, $\alpha_2 = -3.0$, and $L_{\gamma b} = 2.3 \times 10^{51}\,\mathrm{erg\,s^{-1}}$. It implies a smaller local event rate and fewer GRBs at the high-luminosity end. This luminosity function is obtained based on the assumption that the rate of the GRBs follows the star-formation history given by Rowan-Robinson (1999), i.e.,

$$S(z) = \begin{cases} 10^{0.75z} & z < 1, \\ 10^{0.75} & z \geqslant 1. \end{cases} \quad (30)$$

Denoting the differential neutrino number generated by a GRB with luminosity L_γ at local redshift z by $dn_\nu/d\epsilon_\nu$, the injection rate of the neutrinos per unit of time per comoving volume can then be obtained by

$$\Psi(\epsilon_\nu) = \rho(z) \int \frac{dn_\nu}{d\epsilon_\nu}(L_\gamma, \epsilon_\nu) \frac{dN}{dL_\gamma}(L_\gamma) dL_\gamma, \quad (31)$$

where $\rho(z) \equiv \rho_0 S(z)$ is the event rate density in the rest frame. Considering the cosmological time dilation and the particle number conservation, a neutrino with energy ϵ_ν observed at the Earth must be produced at redshift z with energy $(1+z)\epsilon_\nu$ and $\Psi_\nu(\epsilon_\nu^{\rm ob}) d\epsilon_\nu^{\rm ob} = (1+z)\Psi_\nu[(1+z)\epsilon_\nu^{\rm ob}] d\epsilon_\nu^{\rm ob}$. The total observed diffuse neutrino flux can then be integrated over the redshift,

$$\frac{dN_{\rm tot}}{d\epsilon_\nu^{\rm ob}} = \int_0^{z_{\rm max}} \frac{1}{4\pi} \Psi\left[(1+z)\epsilon_\nu^{\rm ob}\right] \frac{c dz'}{H(z')}, \quad (32)$$

where $H(z) = H_0/\sqrt{(1+z)^3\Omega_M + \Omega_\Lambda}$ is the Hubble constant at redshift z. Here, we set $L_{\gamma,\rm min} = 10^{50}\,\mathrm{erg\,s^{-1}}$, $L_{\gamma,\rm max} = 10^{54}\,\mathrm{erg\,s^{-1}}$, and $z_{\rm max} = 8$.

The results of the diffuse neutrino flux are shown in Figure 5. In this plot, we show the diffuse muon-neutrino spectra for the case in which the bulk Lorentz factor of the GRBs follows the inherent relation suggested by Ghirlanda et al. (2012) (solid lines), as described in Section 3, and the case in which a constant Lorentz factor value ($\Gamma = 10^{2.5}$) is assumed for all of the GRBs (dashed lines). The photon spectrum of the GRBs is assumed to be a broken power-law spectrum described by Equation (6), with $\alpha = 1$ and $\beta = 2$, and the break energy of the photon spectrum is calculated from the peak luminosity of the GRBs via the relationship shown in Equation (25). One can see from this plot that using different luminosity functions and the associated source density evolution functions can lead to a very different flux of diffuse neutrinos. The expected flux for the LF-L function slightly exceeds the IC40 upper limit, while, for the luminosity functions of the LF-W and the LF-G, the predicted flux is undetectable even with the one-year operation of the IceCube completed configuration. Particularly, the LF-G function results in a very low flux. This is not only because the local event rate for this luminosity function is much lower, but this is also because many more GRBs are located at the low-luminosity end, contributing a lower neutrino flux than more luminous ones. In order for the diffuse neutrino flux not to exceed the IC40 upper limit, we constrain $\eta_p \lesssim 8$ for the luminosity function of the LF-L. For results in cases where the GRB parameters do not depend on the luminosity, see Murase & Nagataki (2006a), Murase et al. (2006), and Gupta & Zhang (2007).

5. DISCUSSION AND CONCLUSION

The nondetection by the increasingly sensitive detector IceCube has provided some interesting implications for various theoretical predictions of neutrino emission from GRBs. The ICC reported that the IceCube 40-string and 59-string configurations have reached a sensitivity below the theoretical expectation, which, if this is true, would challenge the view that the GRBs could be sources for the UHECRs. However, as illustrated in previous works, we show that the ICC used an overestimated theoretical flux in comparison with the IceCube instrument limit. Therefore, we revisit the analytic calculation of the neutrino flux and consider the realistic photon energy distribution when calculating the number density of the fireball photons (instead of using the bolometric luminosity as the luminosity at the break energy), and we also use the appropriate normalization for the proton flux to evaluate the neutrino flux.

Using the modified formulae, we calculate the expected neutrino flux from the 215 GRBs observed during the 40- and 59-string configurations of the IceCube operations, assuming the same benchmark parameters as those used by the ICC. The flux is about 36% of the 90% CL upper limit, which is consistent with the nondetection of IceCube for the combined data analysis of IC40 and IC59.

The benchmark model assumes constant values for the bulk Lorentz factor, the observed variability time, and the peak luminosity for every burst. Recently, it was suggested that there are correlations between the bulk Lorentz factor and the isotropic energy, as well as between the peak luminosity and the break energy of the photon spectrum. Using such inherent relations to derive the Lorentz factor and the peak luminosity, we

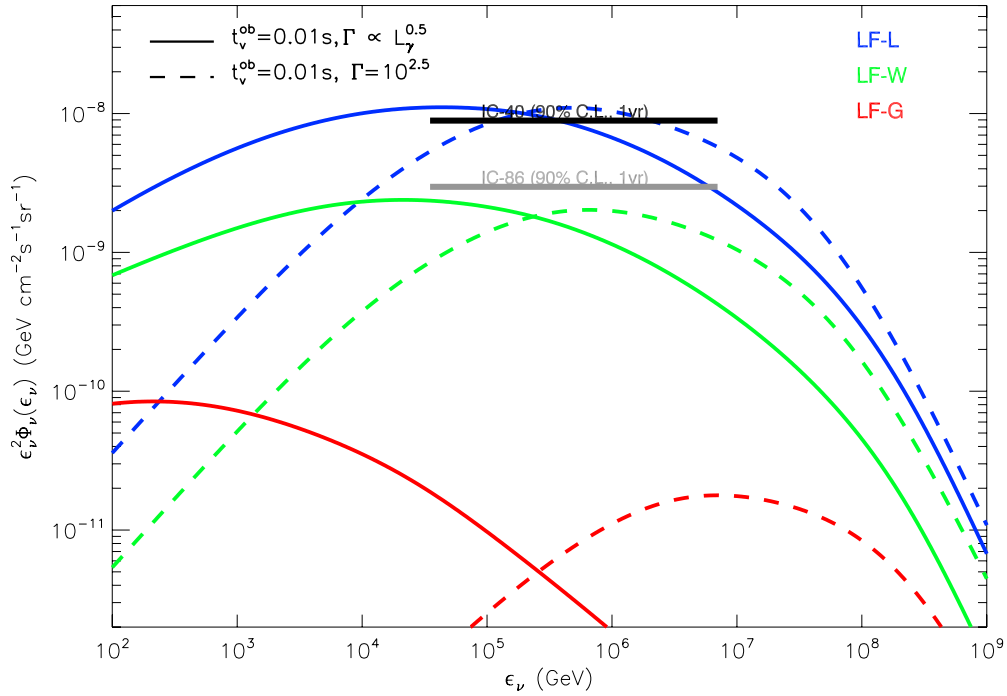

Figure 5. Expected diffuse muon-neutrino flux from the GRBs and the IceCube limits. The blue, green, and red lines represent the fluxes obtained with luminosity functions of Liang et al. (2007), Wanderman & Piran (2010), and Guetta & Piran (2007), respectively. The solid and dashed lines correspond to the different assumptions about the Lorentz factor used in the calculation, but they use the same observed variability timescale $t_v^{\rm ob} = 0.01$ s for the long GRBs and the same baryon-loading ratio $\eta_p = 10$. The black thick solid line is the IC40 upper limit on the diffuse muon-neutrino flux given in Abbasi et al. (2011b), while the dark gray solid line is the upper limit for the one-year observation of the complete IceCube, extrapolated from the upper limit of IC40 via $A_{\rm eff}^{\rm IC86} \simeq 3A_{\rm eff}^{\rm IC40}$ (Karle 2010; Hümmer et al. 2011).
(A color version of this figure is available in the online journal.)

recalculate the neutrino flux and find that the flux adopting these relations exceeds the 90% CL upper limit for the assumption of $t_v^{\rm ob} = 0.01$ s for every long burst. This constrains the baryon ratio to be $\eta_p \lesssim 10$; however, this value could be relaxed if the variability times for most of the GRBs were larger.

We also calculate the cumulative diffuse flux from the GRBs using three different luminosity functions that already exist in the literature. For the luminosity functions of Guetta & Piran (2007) and Wanderman & Piran (2010), the expected flux is below the IceCube upper limit for the case that assumes $\Gamma = 10^{2.5}$ for every burst and the case that considers the inherent relation between Γ and the peak luminosity. However, for the luminosity function obtained in Liang et al. (2007), the expected flux exceeds the IceCube limit for both cases. The nondetection of diffuse neutrinos then constrains the baryon ratio to be $\eta_p \lesssim 8$ in this case.

The GRBs, as well as active galactic nuclei (e.g., Biermann & Strittmatter 1987; Takahara 1990; Berezinsky et al. 2006) and hypernovae/supernovae with relativistic components (Wang et al. 2007; Liu & Wang 2012; Murase et al. 2008) have been proposed as potential sources for the UHECRs. Neutrino detection would provide evidence for cosmic ray protons in the GRBs. On the other hand, the nondetection by the current IceCube cannot yet exclude this connection,[12] because the baryon ratio required for the GRBs to be the sources of the UHECRs is $\eta_p \simeq 5$–10 (Liu et al. 2011) for the local GRB rate of $R \simeq 1\,{\rm Gpc^{-3}\,yr^{-1}}$ (Liang et al. 2007; Wanderman & Piran 2010). Future, more sensitive observations by IceCube or other neutrino telescopes may put tighter constraints on the baryon ratio and may be able to judge the GRB-UHECR connection.

[12] The argument that the GRB-UHECR connection is challenged by the IceCube nondetection in Ahlers et al. (2011) is based on the assumption that the cosmic ray protons are produced by the β-decay of the neutrons from pγ-interactions that escape from the magnetic field.

We are grateful to Peter Redl, Nathan Whitehorn, Svenja Hümmer, Alexander Kusenko, Zhuo Li, and Juan Antonio Aguilar for their valuable discussions. This work is supported by the NSFC under grants 10973008, 10873009, and 11033002, the 973 program under grants 2009CB824800 and 2007CB815404, the program of NCET, the Jiangsu Province Innovation for PhD candidate CXZZ11_0031, the Fok Ying Tung Education Foundation, and the Global COE Program. S.N. acknowledges support from the Ministry of Education, Culture, Sports, Science and Technology (No. 23105709), the Japan Society for the Promotion of Science (No. 19104006 and No. 23340069), and the Global COE Program "The Next Generation of Physics, Spun from University and Emergence from MEXT of Japan." K.M. is supported by CCAPP at OSU and JSPS.

REFERENCES

Abbasi, R., Abdou, Y., Abu-Zayyad, T., et al. 2010, ApJ, 710, 346
Abbasi, R., Abdou, Y., Abu-Zayyad, T., et al. 2011a, Phys. Rev. Lett., 106, 141101
Abbasi, R., Abdou, Y., Abu-Zayyad, T., et al. 2011b, Phys. Rev. D, 84, 082001
Ahlers, M., Gonzalez-Garcia, M. C., & Halzen, F. 2011, Astropart. Phys., 35, 87
Atoyan, A., & Dermer, C. D. 2001, Phys. Rev. Lett., 87, 221102
Baerwald, P., Hümmer, S., & Winter, W. 2011, Phys. Rev. D, 83, 067303
Berezinsky, V., Gazizov, A. Z., & Grigorieva, S. I. 2006, Phys. Rev. D, 74, 043005
Biermann, P. L., & Strittmatter, P. A. 1987, ApJ, 322, 643
Dai, Z. G., & Lu, T. 2001, ApJ, 551, 249
Dermer, C. D. 2002, ApJ, 574, 65

Dermer, C. D., & Atoyan, A. 2006, New J. Phys., 8, 122
Ghirlanda, G., Nava, L., Ghisellini, G., et al. 2012, MNRAS, 420, 483
Giannios, D. 2010, MNRAS, 408, L46
Guetta, D., Hooper, D., Alvarez-Mun-Iz, J., Halzen, F., & Reuveni, E. 2004, Astropart. Phys., 20, 429
Guetta, D., & Piran, T. 2007, J. Cosmol. Astropart. Phys., JCAP07(2007)003
Gupta, N., & Zhang, B. 2007, Astropart. Phys., 27, 386
Hümmer, S., Baerwald, P., & Winter, W. 2011, arXiv:1112.1076
Karle, A. for the IceCube Collaboration 2010, arXiv:1003.5715
Kashti, T., & Waxman, E. 2005, Phys. Rev. Lett., 95, 181101
Kumar, P., & Narayan, R. 2009, MNRAS, 395, 472
Liang, E.-W., Yi, S.-X., Zhang, J., et al. 2010, ApJ, 725, 2209
Liang, E., Zhang, B., Virgili, F., & Dai, Z. G. 2007, ApJ, 662, 1111
Liu, R. Y., & Wang, X. Y. 2012, ApJ, 746, 40
Liu, R.-Y., Wang, X.-Y., & Dai, Z.-G. 2011, MNRAS, 418, 1382
Li, Z. 2012, Phys. Rev. D, 85, 027301
Lv, J., Zou, Y.-C., Lei, W.-H., et al. 2011, arXiv:1109.3757
Mücke, A., Engel, R., Rachen, J. P., Protheroe, R. J., & Stanev, T. 2000, Comput. Phys. Commun., 124, 290
Mucke, A., Rachen, J. P., Engel, R., Protheroe, R. J., & Stanev, T. 1999, PASA, 16, 160
Murase, K. 2007, Phys. Rev. D, 76, 123001
Murase, K. 2008, Phys. Rev. D, 78, 101302
Murase, K., Asano, K., Terasawa, T., & Mészáros, P. 2012, ApJ, 746, 164
Murase, K., Ioka, K., Nagataki, S., & Nakamura, T. 2006, ApJ, 651, L5
Murase, K., Ioka, K., Nagataki, S., & Nakamura, T. 2008, Phys. Rev. D, 78, 023005
Murase, K., & Nagataki, S. 2006a, Phys. Rev. Lett., 97, 051101
Murase, K., & Nagataki, S. 2006b, Phys. Rev. D, 73, 063002
Nagataki, S., Kohri, K., Ando, S., & Sato, K. 2003, Astropart. Phys., 18, 551
Nakar, E., & Piran, T. 2002, ApJ, 572, L139
Narayan, R., & Kumar, P. 2009, MNRAS, 394, L117
Paczynski, B., & Xu, G. 1994, ApJ, 427, 708
Particle Data Group, Eidelman, S., Hayes, K. G., et al. 2004, Phys. Lett. B, 592, 1
Porciani, C., & Madau, P. 2001, ApJ, 548, 522
Rees, M. J., & Meszaros, P. 1994, ApJ, 430, L93
Rowan-Robinson, M. 1999, Ap&SS, 266, 291
Takahara, F. 1990, Prog. Theor. Phys., 83, 1071
The IceCube Collaboration 2011, arXiv:1111.2741
Vietri, M. 1995, ApJ, 453, 883
Wanderman, D., & Piran, T. 2010, MNRAS, 406, 1944
Wang, X. Y., & Dai, Z. G. 2009, ApJ, 691, L67
Wang, X.-Y., Razzaque, S., Mészáros, P., & Dai, Z.-G. 2007, Phys. Rev. D, 76, 083009
Waxman, E. 1995, Phys. Rev. Lett., 75, 386
Waxman, E., & Bahcall, J. 1997, Phys. Rev. Lett., 78, 2292
Waxman, E., & Bahcall, J. N. 2000, ApJ, 541, 707
Yonetoku, D., Murakami, T., Nakamura, T., et al. 2004, ApJ, 609, 935
Zhang, B., & Yan, H. 2011, ApJ, 726, 90